AIAA JOURNAL
Vol. 36, No. 3, March 1998

Flight Results from the Middeck Active Control Experiment (MACE)

David W. Miller,* Jonathan P. How,† Mark E. Campbell,‡ Simon Grocott,§
Ketao Liu,¶ Roger M. Glaese,** and Timothy Tuttle††
Massachusetts Institute of Technology, Cambridge, Massachusetts 02139

The middeck active control experiment (MACE) was designed as a Space Shuttle flight experiment to demonstrate high authority active structural control in zero-gravity (0-*g*) conditions based on analysis, ground testing, and on-orbit control redesign. MACE is a multidisciplinary project that is at the forefront of flexible structural control. MACE was first flown on STS-67 in March 1995, and a summary of the program objectives and mission experimental results is provided.

I. Introduction

THE middeck active control experiment (MACE) is a Space Shuttle flight experiment that flew on Space Transportation System (STS) 67 in March 1995. MACE was designed through a cooperative effort between academia, industry, and NASA to investigate approaches for achieving high-precision pointing and vibration control of future spacecraft and satellites. In the past, control performance has been limited by flexibility in the system due to a phenomenon known as control-structures interaction.[1] Overcoming this problem requires a multidisciplinary approach that combines state-of-the-art capabilities in modeling and model updating, system identification, uncertainty model development, controller analysis, and robust control synthesis. This paper presents a set of techniques that were developed to address these issues for MACE.

Control-structures interaction (CSI) occurs when control detrimentally interacts with flexibility in a system. Such interaction is caused by mismodeling or lack of consideration for flexibility. The U.S. space program has a history of problems related to CSI, which have ranged from degrading spacecraft performance to causing catastrophic loss of the system.[2] Problems with spacecraft flexibility started as early as the first U.S. satellite, Explorer I (1958). Unexpected energy dissipation in the flexibility of the four whip antennas on the spin-stabilized satellite caused it to tumble. Attitude oscillation caused by the control system interacting with boom and solar panel flexibility occurred on OGO III (1966), OVI-10 (1966), DMSP (1972), and Mariner 10 (1973), which was almost lost. Thermal warping and snapping proved to be a major source of agitation in Alouette I (1962), Explorer XX (1964), OGO IV (1966), Voyager (1977), and Landsat (1982, 1984). In current systems, the pointing control system for the Hubble Space Telescope was initially limited due to thermally induced disturbances originating in the solar arrays.[3]

The contemporary solution to the CSI problem has been to analyze system dynamics and limit the bandwidth of the control so as to not include flexibility. Thus, flexibility has typically placed a limit on the performance of systems, which is particularly true for space applications where rigidizing structures are obtained at high launch costs. The MACE program was developed to investigate controlled structures technology (CST) as a means for controlling rather than avoiding flexibility in space systems, thereby penetrating this artificial performance barrier. The overall objective of the MACE program was to develop a set of CST tools that allow designers of future spacecraft that cannot be tested on the ground in a sufficiently realistic 0-*g* simulation to have confidence in the eventual on-orbit performance of such spacecraft.[4] In other words, the goal was to make CST work predictably and effectively on a spacecraft that has dynamics that change when it is launched into space. Specifically, this overall objective was separated into the following mission objectives: 1) to understand how gravity affects the open- and closed-loop ground test results, 2) to develop tools to predict the on-orbit behavior, 3) to quantify the accuracy to which the behavior can be predicted, 4) to measure the open- and closed-loop behavior on orbit and update the control system, and 5) to quantify the performance improvement that can be achieved through both prelaunch and on-orbit updated control designs.

This paper discusses each of these objectives, how they have been met through the MACE mission, and the primary lessons that have been learned throughout the program. In the process, a complete set of flight results from MACE are presented to demonstrate how the final conclusions were reached. These discussions will also demonstrate that, although there have been many studies of practical control of flexible systems and a very large number of CSI test facilities developed (see Refs. 5 and 6 and the citations therein), the MACE program is unique in its extensive implementation of on-orbit experiments. Although a summary of the CST tools developed for MACE is presented in this paper, a more complete discussion is given in Refs. 7–10.

The following section provides a brief introduction to the MACE hardware and the on-orbit operations. This is followed by three sections that discuss the five primary objectives just listed, within the context of system modeling, performance analysis, and control design. The final section then summarizes the main observations from the MACE flight results and how they impact future spacecraft missions.

II. Hardware Design and Description

The MACE hardware was designed to satisfy many different, and often conflicting, requirements. The hardware had to provide a

Received March 8, 1997; revision received Oct. 31, 1997; accepted for publication Nov. 9, 1997.

*Principal Research Scientist, Space Engineering Research Center, Department of Aeronautics and Astronautics, Room 37-371, 77 Massachusetts Avenue. Member AIAA.

†Postdoctoral Associate, Space Engineering Research Center, Department of Aeronautics and Astronautics; currently Assistant Professor, Department of Aeronautics and Astronautics, Stanford University, Stanford, CA 94305. Member AIAA.

‡Research Assistant, Space Engineering Research Center, Department of Aeronautics and Astronautics; currently Assistant Professor, Department of Aeronautics and Astronautics, University of Washington, Box 352400, Seattle, WA 98195-2400. Member AIAA.

§Research Assistant, Space Engineering Research Center, Department of Aeronautics and Astronautics; currently Intermediate Member of Technical Staff, SPAR Space Systems, Brampton, ON, Canada.

¶Postdoctoral Associate, Space Engineering Research Center, Department of Aeronautics and Astronautics; currently Member of the Technical Staff, Hughes Space and Communications Company, El Segundo, CA 90245. Member AIAA.

**Research Assistant, Space Engineering Research Center, Department of Aeronautics and Astronautics; currently Project Engineer, CSA Engineering, Palo Alto, CA 94303. Member AIAA.

††Research Assistant, Space Engineering Research Center, Department of Aeronautics and Astronautics; currently Research Fellow, Massachusetts Institute of Technology, Lincoln Laboratory, Lexington, MA 02173.

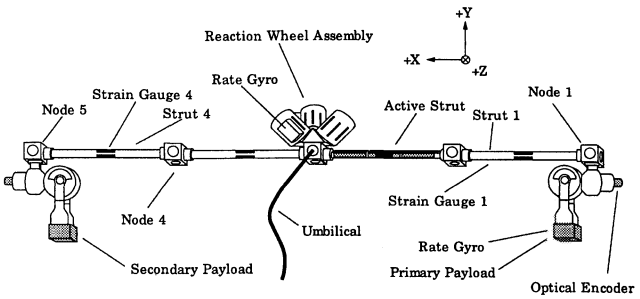

Fig. 1 MACE configuration I schematic.

challenging, interactive, CSI/CST test article and control laboratory, but this had to be accomplished within the very tight constraints on volume, weight, power, and crew time required of a Space Shuttle middeck experiment. The hardware designed has three distinct parts: 1) the multibody platform (MBP) test article, 2) the experiment support module (ESM), and 3) the Ku-band interface system (KIS). The ESM provided all electronics as well as data storage for MACE. The KIS provided the capability for uplink and downlink of data.

The MBP was chosen to be dynamically representative of a precision-controlled, high payload mass fraction spacecraft, such as Earth-observing platforms, with multiple, independently pointing or scanning payloads.[11] The following five major requirements were placed on the MBP design to ensure that there was sufficient control-structures interaction to be representative of problems experienced on previous spacecraft (and anticipated on future ones), thereby allowing the development and validation of new technologies, and sufficient flexibility to include additional tests within the confines of the Space Shuttle middeck.

1) The fundamental bending frequency of the test article must be below 2 Hz and must possess a minimum of nine flexible modes below 60 Hz.

2) It must be reconfigurable into more complex and challenging configurations.

3) MACE must be able to be assembled in under 30 min by one crew member.

4) Unassembled, MACE must be small enough to fit in a middeck locker.

5) For safety purposes, it must structurally withstand, with proper margins, all potential dynamic instabilities.

These requirements were met by adopting a modular, electrically integrated design shown in Fig. 1. The test article consists of a segmented flexible structural bus with integral power and data connections. A two-axis gimballed payload containing two-axis rate gyros for inertial pointing angle determination is mounted at each end of the bus. A three-axis reaction wheel assembly (RWA), mounted in the center of the bus, provides attitude control torques. In addition, a two-axis piezoelectric bending strut is located next to the RWA on the primary end of the structure. Each strut is instrumented with strain gauges measuring bending strain in two axes. An optical encoder is mounted on each gimbal axis to measure the angular rate and displacement of the payload relative to the bus. Attached to the RWA are three rate gyros to measure inertial attitude of the bus and three tachometers to measure the speed of the reaction wheels. The resulting structure had 15 modes below 60 Hz.

Although not shown, a second "L" configuration of MACE (configuration II) was also used on orbit. The second configuration was similar to the first in that it shared all hardware components of the test article, with the exception of one node between strut 1 and the active strut. The second configuration utilized a node that allowed strut 1 to be attached at a 90-deg angle to the bus, thereby creating the L shape. The L configuration was only tested on orbit and not on the ground, thus allowing MACE to examine the concept of designing and controlling a spacecraft that can only be tested on the ground in a configuration that is distinct from its eventual use. Details of the results of this configuration are given in Ref. 9.

A power and data umbilical is attached at the center node to the ESM. The ESM contains the real-time control computer, which supports all 20 sensors and 9 actuators and is capable of running an 80-state compensator at a sample rate of 500 Hz. Data storage was accomplished with optical disks that could be replaced on orbit as needed. In addition, the success of the program also rested on the ability to downlink data and uplink controllers to the middeck (see objective 5). The KIS was developed for MACE because there was no existing high data rate transmission capability from the middeck.

III. Flight Operations

MACE was a secondary middeck payload on the STS-67 mission in March of 1995, behind the ASTRO-2 telescopes. The experiment was operated by Commander Stephen Oswald and Pilot William Gregory on 14 of the 16 days of the mission, much more than the 6 days planned in the mission time line. On-orbit testing consisted of implementing experiments of three different varieties: identification, control, and input shaping protocols.[10] To satisfy objective 2, at various phases of the mission, data were downlinked using the KIS to redesign the experiments. These new experiments were then uplinked, using the KIS, for implementation on subsequent days. Commander Oswald implemented over 60 identification, 240 preprogrammed control, 180 redesigned control, 55 preprogrammed input shaping, and 35 redesigned input shaping protocols.

Two important aspects of the flight hardware were the use of tethers and gimbal servos. The MBP was tethered in the middeck by three very flexible elastics. It became apparent during the mission that tethering was necessary to keep the test article centered in the middeck, particularly during thruster firings. Although the use of tethers was possible, the specific application of the tethers was not known before flight because it was at the discretion of the astronauts. (Note that a few experiments were also implemented while MACE was free floating.) Second, four gimbal servocontrollers, which caused the gimbal angles relative to the bus to track command signals, were used in two cases. First, a low-bandwidth servo (one-tenth the frequency of the first flexible mode) was used as the standard industry practice for pointing control because it avoided interaction with structural flexibility. A second set of higher-bandwidth servocontrollers were also used to perform the nominal payload pointing with respect the spacecraft bus. The overall pointing performance was then improved by designing higher-authority CST controllers that reduced the structural vibrations of the spacecraft bus.

IV. Modeling

Attaining a high level of performance improvement in the pointing control of flexible systems requires not only an advanced control methodology but also an accurate model of the dynamics. Thus, a two-pronged modeling strategy was used. This approach used analytic models to develop predictions of the on-orbit dynamics and identified models based on the measured on-orbit behavior. Measurement models are typically more accurate than analytical models because they are formed by fitting the experimental data. Although measurement models accurately reproduce the measured behavior, they do not necessarily result in a good model of the internal mechanisms of the system. For structures whose eventual application is in space, no 0-g experimental data exist before flight to form a measurement model. Therefore analytical modeling techniques must be used to model the structure while it is suspended and tested on the ground. In addition to the inaccuracies of analytical modeling, however, gravity and the suspension also modify the dynamics of the structure from its 0-g behavior. Therefore these changes must also be modeled. It is the demonstration of these two modeling techniques on MACE that satisfies objectives 1, 2, and 4 in the Introduction.

A. Analytical Modeling and Gravity Effects

MACE analytical models were derived using the finite element (FE) method. The models are derived from the physical equations of motion and, as such, should capture the internal mechanics and physics of the system. However, it is often extremely difficult to make analytical models accurately agree with the measured input and output behavior of the system. In fact, ground tests before flight indicated that the initial FE model had very large errors when compared with the experimental data. To improve the modeling accuracy, the physical parameters of the model, such as Young's modulus, density, and cross-sectional area, were updated using ground experimental data and a least-squares algorithm.[12] Physical parameters

rather than modal parameters of the model must be updated because there would be no explicit way to remove the gravity and suspension effects to arrive at a 0-g prediction if the latter were used. Once the 1-g model had achieved a desired level of accuracy (usually determined by the robust control methods and 1-g testing results), the gravity and suspension effects were then removed from the model. This model, the final 0-g model, represented the best prediction of the 0-g behavior of the structure before flight because the 1-g model has been correlated with the only available set of data.

Other programs[13] have looked at the 1- to 0-g transition, but no design rules of thumb are available. Therefore, the first objective was to understand how gravity affected the modeling of a structure and the impact of those effects on control design and performance. Some of the gravity effects influence the entire structure, such as sag, predeformation, and preloading of structural members, resulting in an increase in modal frequency. Others affect components of the structure, such as pendular effects on articulating appendages and stiffening of rigid-body behavior. In both of these effects, zero-frequency rigid-body modes are stiffened to nonzero frequencies in a manner similar to the simple pendulum. All of these effects corrupt the correlation between a structure's 0-g behavior and any ground tests that might be performed. A detailed analysis of these effects can be found in Ref. 14.

Modeling the suspension, prestress, and sag effects revealed perturbations in the pendulum, suspension violin, and structural modes. Figure 2 compares the 1- and 0-g FE models for one transfer function. The actuator is the secondary gimbal, and the sensor is the payload rate gyro in the appropriate directions, as shown in Fig. 1. Figure 2 shows that the low-frequency pendulum modes are eliminated when the gravity effects are removed. Likewise, the transverse violin modes of the 1-g suspension cables, which are interspersed throughout the structural mode region, appear only in the 1-g model.

Table 1 shows the variation of the modal frequencies for the FE model between 1 and 0 g and the errors in the 0-g FE model when compared with the very accurate measurement model. These results show that gravity has a significant effect on the modal frequencies, with shifts of more than 10%. Note that there are fewer modes in 0 g than in 1 g, because the gravity and suspension stiffen the rigid-body modes and create new suspension modes. An examination of the 0-g frequency errors shows that most of the errors are 3% or less, leading to the conclusion that, except for a few modes, the analytical modeling technique performed quite well.

These ground and flight results indicate that gravity impacts the FE-based 0-g control design in key ways.

1) The model updating process is complicated. Without the ability to test the spacecraft in 0 g before flight, all analytical model refinement must be done using available ground test data. Because the gravity effects introduce suspension modes and structural mode perturbations, the ground model is much more complex and therefore more difficult to model accurately.

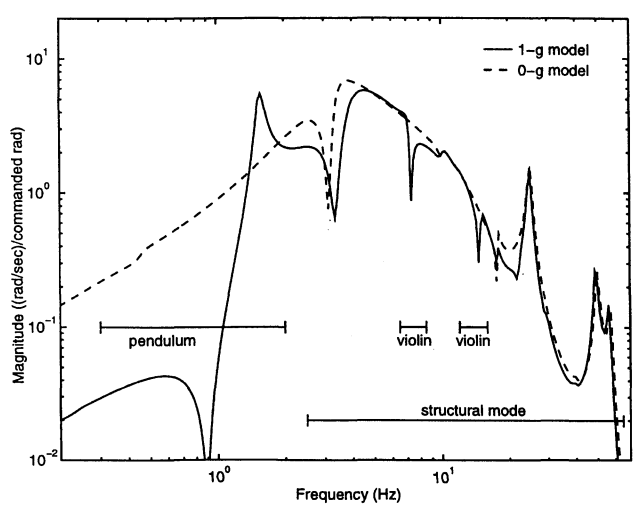

Fig. 2 Comparison of 1- and 0-g models: x axis; secondary gimbal X to payload rate gyro X.

Table 1 Modal frequencies for the 1- and 0-g FE models, 1- to 0-g changes, and 0-g frequency errors

Description of mode	FE model, Hz 1 g	FE model, Hz 0 g	Change, %	0-g error, %
Suspension rotary pendulum	0.24	—	—	—
Suspension tilt	0.44	—	—	—
Suspension compound pendulum	1.55	—	—	—
First vertical bending	2.13	2.10	−1.4	−2.1
First horizontal bending	3.74	3.31	−12.7	−0.1
Gimbal pendulum	3.38	3.07	−10.1	−1.4
Gimbal pendulum	5.26	5.11	−2.9	−13.7
Gimbal pendulum	5.32	5.37	0.9	−4.3
Gimbal pendulum	5.50	5.47	−0.5	−2.7
First violin	7.26	—	—	—
First violin	7.34	—	—	—
Second vertical bending	8.98	8.76	−2.5	1.5
Second horizontal bending	10.12	10.09	−0.3	−1.5
Third vertical bending	10.45	10.11	−3.4	3.7
First violin	11.65	—	—	—
Third horizontal bending	14.09	14.07	−0.2	−3.1
Second violin	14.68	—	—	—
Second violin	14.71	—	—	—
Fourth vertical bending	15.82	15.68	−0.9	1.6
Fourth horizontal bending	17.81	17.84	0.1	1.3

2) There were significant gravity perturbations to structural frequencies, the largest being a 10% frequency shift and the average frequency shift being 2%. Of course, the large uncertainty in these changes before flight significantly impacted the control design process.

3) Poor repeatability of the suspension system in 1 g complicated the control design and model validation/updating processes.

B. Measurement Modeling

The on-orbit measurement model was created using data that were downlinked during the mission. A frequency domain technique was used because the stability and performance of a control system can be efficiently assessed in the frequency domain. The identification was performed using the integrated frequency-domain observability range space extraction and least-squares parameter estimation technique,[15] a highly accurate technique for low-order model identification. It consists of an initial stage of model identification using frequency-domain observability range space extraction and iterative refinements using balanced model reduction and least-squares parameter estimation techniques. The final model generated by this technique is usually highly accurate and of low order.

The identification experiments themselves must be well planned to achieve accurate measurement models. This was difficult for MACE because the identification experiments were also complicated by the transition from 1 to 0 g. Because of the removal of the suspension and gravity, the 1- and 0-g systems were sufficiently different that the same excitation amplitudes and sample lengths could not be used. Because the analytical model captures the input and output characteristics of the hardware, it was used to assist in the design of the identification experiments. This approach was very successful in designing all of the experiments such that the output signals were strong enough to create accurate measurement models, without generating input signals that saturated the actuators.

C. Zero-Gravity Validation

The experimental results for configuration I show that both the FE model and measurement model are very accurate in the sense that they match the 0-g data quite well above 0.2 Hz (Fig. 3). Figure 3 shows 1 of at least 25 frequency responses that are relevant for the control results in Sec. VI. Note that the measurement model is so accurate that the frequency response is almost indistinguishable from the experimental data points.

There were, however, two issues in the modeling process that became important during the flight. The first is several missing modes in the analytical model, as shown by examining the low-frequency portion of Fig. 3. The measurement model captures the mode at 0.14 Hz quite well, but the analytical model does not. Figure 3 also shows that neither of these two models captures the mode below

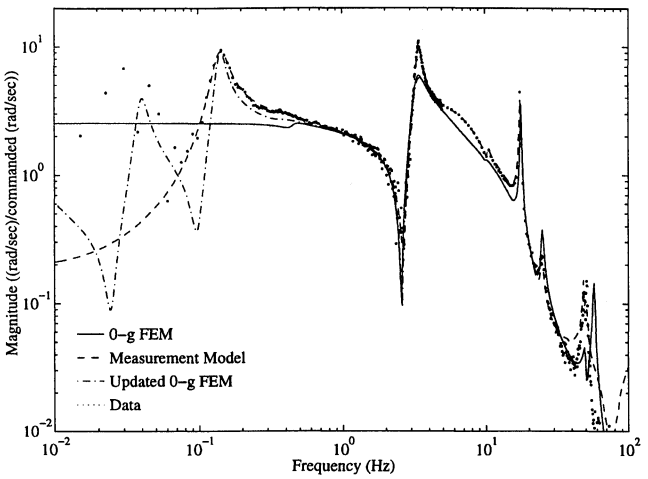

Fig. 3 Comparison of the initial and updated 0-*g* FE models and measurement model with 0-*g* data for configuration I: reaction wheel *X* to payload rate gyro *X*.

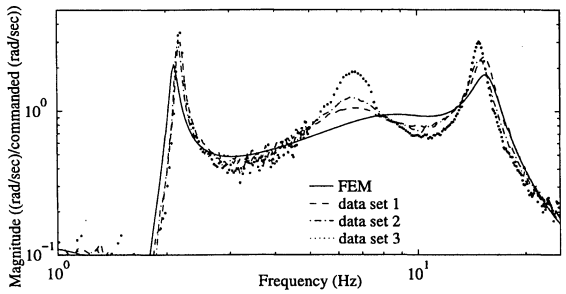

Fig. 4 Frequency responses showing the effects of the nonlinearity.

0.1 Hz. These low-frequency modes are caused by the umbilical and soft tethers used to position the test article in the Space Shuttle's middeck. Although the flight plan called for the test article to be free-floated without the need for tethers if possible, on-orbit experience showed it was not possible. The tethers were assumed to be at frequencies less than 0.01 Hz and were therefore omitted from the 0-*g* analytical model and treated in the control design process. The umbilical, on the other hand, was included in the model but in the wrong physical configuration. As is shown in Sec. V, this mismodeling of the low-frequency tether and umbilical modes caused instability in several of the preprogrammed controllers. Downlinked video was used to determine the configuration of the tethers and umbilical on the middeck, and the 0-*g* FE model was updated. The updated 0-*g* FE model (Fig. 3) captures the suspension mode at 0.14 Hz very well and roughly captures the behavior below 0.1 Hz. This improved model was successfully used to redesign FE-based controllers during the mission.

The second issue involved a slight amplitude nonlinearity in the system that proved to be quite important, as discussed in the following analysis and control design sections. The flight results obtained during the mission clearly indicated that the measurement models did not provide as accurate a model of the system dynamics as suggested by the comparison with the experimental data, especially in closed loop. Postflight analysis indicated that this was primarily due to a nonlinear effect associated with friction in the gimballing payloads. Figure 4 shows a comparison of experimental frequency responses due to decreasing excitation levels (from 1 to 3) from a reaction wheel input to a collocated rate gyro. The nonlinearity predominantly modifies the 5–12-Hz frequency range. At low excitation amplitudes (data set 3), friction dominates the gimbal response, causing an apparent locking of the gimbals and thereby increasing the frequency (and reducing the damping) of modes that are tightly controlled by the gimbal servos. In addition, the apparent gain around 10 Hz is lower. The postflight analysis indicated, however, that the system dynamics in closed loop, especially at 10 Hz, were closer to the FE model because the controller and high-frequency disturbances created an effective dither in the gimbals, thus preventing the system from operating in the locked condition. Therefore, although the identified model added dynamics to fit the nonlinear response (primary gimbal locked) with a linear model, which it did quite well, the actual response was more accurately represented by the FE model. The closed-loop implications of the modeling errors shown in Fig. 4 are discussed subsequently.

V. Control Analysis

As discussed, MACE was designed to investigate the modeling and control design issues associated with changing the operational environment of a flexible spacecraft from 1 to 0 *g*. As such, errors in the prediction of the 0-*g* dynamics were expected to exist in the control design models, and so analysis played a very important role in the control design process. For most systems, the primary analysis issues are how to model the errors in the system dynamics and which analysis tools to use to test for robust stability and performance. As is shown, the complexity of the analysis problem for MACE is compounded by the large number of real parametric uncertainties that strongly influenced the performance and the inability to predict these uncertainties before flight.

There were two distinct phases of control design for the MACE mission. In the first, controllers were designed before flight based on a FE model of the system. In the second, controllers were designed during the flight based on either the FE model or models derived from system identification (ID) measurements taken during the mission. Because open-loop data were available during the flight, this additional information was used for control analysis during the mission. As a result, two analysis procedures were developed to be performed with and without the use of open-loop data. This section demonstrates the effectiveness of these analysis techniques and, in the process, addresses objectives 2 and 3, which ask how well the on-orbit behavior can be predicted using analysis and ground testing.

A. Analysis with Open-Loop Data

The procedure for control system analysis using open-loop data developed for MACE is shown in Ref. 16 and summarized here. With open-loop data available in the form of a transfer function matrix

$$G(j\omega) = \begin{bmatrix} G_{zw}(j\omega) & G_{zu}(j\omega) \\ G_{yw}(j\omega) & G_{yu}(j\omega) \end{bmatrix} \tag{1}$$

where z are the performance outputs, y are the sensor outputs, w are the disturbance inputs, and u are the actuator inputs, it is possible to "close the loop" using these data and the frequency response of the controller. The model and data predictions can then be overlaid to get a prediction of the closed-loop performance, stability, and proximity to instability.

The system performance is analyzed using the closed-loop state cost, whereas the closed-loop stability is assessed using the multivariable Nyquist test.[17] For closed-loop stability, the number of counterclockwise encirclements of the critical point $(-1, 0)$ of the multivariable Nyquist function

$$H_n(j\omega) = -1 + \det[I + G_{yu}(j\omega)K(j\omega)] \tag{2}$$

must equal the number of unstable poles in the open-loop system and compensator. In a single-input/single-output system, the Nyquist function additionally provides the concepts of gain and phase margin, but these cannot be obtained from the Nyquist function for multi-input/multi-output systems. However, the maximum singular value of the sensitivity transfer function, where

$$\bar{\sigma}[S(j\omega)] = \bar{\sigma}\left\{[I + G_{yu}(j\omega)K(j\omega)]^{-1}\right\} \tag{3}$$

gives a direct measure of the proximity to singularity of the system and is the third criterion used for prediction. In particular, if a model-based and a data-based calculation of $\bar{\sigma}[S(j\omega)]$ strongly disagree and $\bar{\sigma}[S(j\omega)] > 1$ for either case, the controller is not very robust to model errors and could possibly destabilize the actual system.

In general, the controllers designed and analyzed on the ground using the open-loop data analysis performed quite well.[16] This open-loop data analysis was then performed during the redesign period of the mission. These experimental results (discussed in detail in the following sections) led to the conclusion that the analysis procedures

based on the open-loop data were very effective for predicting the stability and performance problems of the controllers implemented on orbit. There were, however, a few exceptions. Four controllers (out of nearly 100) that were approved by this analysis destabilized the actual system. In all four cases, the instability occurred at approximately 10 Hz, and during postflight analysis the cause was determined to be the nonlinearity discussed earlier.

In particular, it was determined through analysis after the mission that one transfer function was critical in predicting the 10-Hz instability. Figure 4 shows this transfer function for the FE model and for each of three data sets with decreasing input amplitude. The postflight analysis revealed that because of the inability of certain inputs to overcome friction elsewhere in the test article, the 5–12-Hz range for this transfer function is quite sensitive to the input disturbance amplitude. As shown, the damping decreases for decreasing input levels (from 1 to 3), thus increasing the response at 7 Hz and decreasing the response at 10 Hz. In closed loop, however, the system dynamics near 10 Hz were more accurately captured by the higher gain of the FE model. Therefore, because the measurement model gain was lower than the actual system near 10 Hz, the actual loop gain for these controllers on the actual system in the 10-Hz region was larger than predicted. The postflight analysis confirmed that these gain changes (shown in Fig. 4) were sufficient to destabilize these four controllers. In addition, the postflight analysis showed that the nonlinearity, although still strong in 1 g, did not limit the 1-g closed-loop results.

It was quite clear during the mission that the FE model more accurately represented the response of the system in closed loop near 10 Hz, and so it was used to analyze the measurement-model-based controllers. It is noted, however, that the nonlinear nature of the problem was not well understood until after the mission when more identification data sets were available. An example of this analysis for one of the destabilizing controllers is shown in Fig. 5a, which plots $H_n(j\omega)$ as magnitude vs phase (for stability, H_n must pass below all of the critical points, ×), and Fig. 5b, which plots the singular values of the sensitivity transfer function. The results show that there is no indication from the analysis on the original data, through either encirclements or large sensitivity in the 5–12-Hz frequency range, that a stability or performance problem would occur. This result is consistent with the open-loop data analysis during the mission. Furthermore, the measurement-based model predictions were identical to the data predictions because of the close fit of the model to the data. However, the same analysis performed on the more accurate representation of the dynamics provided by the FE model clearly shows that this controller is not robust. Figure 5b shows that the sensitivity peaks at approximately 20 near 10 Hz compared with

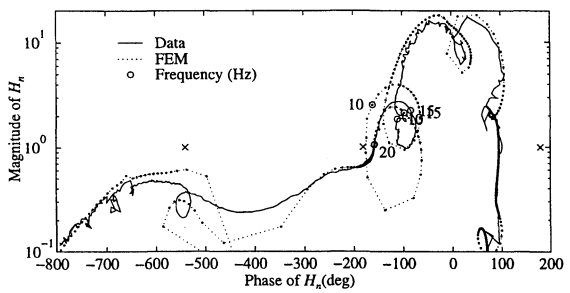

a) Nyquist function plotted magnitude vs phase

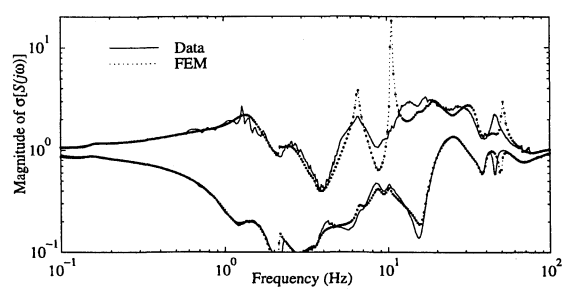

b) Singular values of sensitivity transfer function

Fig. 5 Plots for stability prediction using FE model and open-loop data.

2 predicted by the data. In summary, a few data predictions were not successful during the mission because the system response was corrupted by the friction nonlinearity, whereas the analysis using the FE model provided some key insights into these problems.

B. Analysis Without Using Open-Loop Data

Before flight, open-loop 0-g data were not available, and so a different analysis method had to be used. An alternative method was developed[8,18] that relies on a model of the type and size of the system uncertainty. For structural systems such as the MACE test article, the most significant model errors and uncertainties are typically in the frequency and damping of the flexible modes. Thus, for the MACE project, it was necessary to predict the frequency and damping uncertainties in 0 g based on 1-g testing and then to analyze the closed-loop system to check for stability and performance over the predicted range of uncertainty.

The process that was developed uses the mean and variance of the difference between measured and FE model frequencies and damping ratios in 1 g to provide a measure of the modeling error and variability of the structure on the ground. This 1-g uncertainty model was then combined with both the 1-g and 0-g FE models to predict the 0-g uncertainty model.[18] The approach uses a perturbation expansion of the generalized structural eigenvalue problem to convert the mean and variance of the frequency uncertainties to mass and stiffness perturbations. These physical uncertainties are then mapped into 0 g using the FE model to predict mean errors and bounds for the on-orbit frequencies. Damping predictions are more tenuous and difficult to predict, however. Therefore, large conservative variances were used to create the damping bounds.

The uncertainty model was then used in a mixed-μ analysis[19,20] to determine robust stability and performance of the system over the full range of parameters in the uncertainty model. The uncertainty set typically included 20 real parametric uncertainties (frequencies and damping ratios of 10 modes) and one complex uncertainty to ensure the problem is continuous in the problem data.[19] Motivated by our experience with the open-loop data analysis, which indicated that significant variation between model and data predictions of $S(j\omega)$ showed a lack of robustness, the complex block was chosen to be a weighted sensitivity transfer function to give a measure of the proximity to instability of the closed-loop system. The weight was normalized by the maximum singular value of the nominal sensitivity and included a scaling factor α that determined the maximum allowable change in the perturbed sensitivity. Ground-based experimental tests indicated that $\alpha = 2$ led to good closed-loop stability and performance, and so this value was used in the analysis of the preprogrammed controllers. Therefore, the μ test provided information similar to that of the open-loop data analysis but used the predicted uncertainty model rather than the data.

One possible drawback of this approach is the conservatism of the analysis technique. First, μ itself is not calculated but rather upper and lower bounds, which can be conservative for a large number of uncertainties. Second, independent variations of all frequencies and damping ratios are assumed, but because correlation probably exists between the modeling errors, conservatism is again introduced. However, given a model of the 0-g uncertainty, this analysis approach is well suited to preprogrammed operations during which data are not available. Note that at the time, the μ analysis could not be used to directly test the robust $\mathcal{H}_2$ performance of the system, but this is now feasible given the results in Refs. 21 and 22.

There was also a question of how the uncertainty model was to be used with the μ analysis. The control design model could be shifted by the mean predictions and evaluated using only the predicted bounds. Because shifting the design model by the predicted mean errors could also alter the zero structure of the feedback control loops and the confidence in the predicted uncertainty model was not high before flight, the FE model itself was used as the design model for most of the controllers. The μ analysis then used a set of bounds that were expanded to cover the mean plus the 3σ variations in the parameters. This larger uncertainty introduces more conservatism into the mixed-μ analysis but provides more confidence in the preprogrammed controllers.

With the flight data now available, the accuracy of the uncertainty model can be evaluated. Figure 6 compares the predicted and

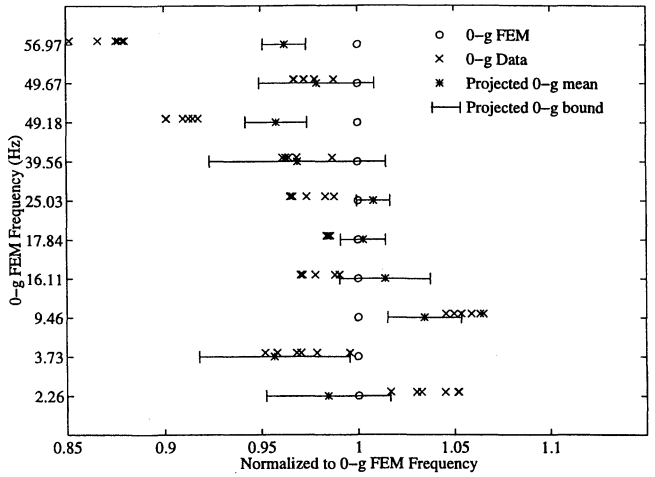

Fig. 6 0-g validation of the FE model and uncertainty model frequencies.

measured frequencies. The FE model frequency (o) and uncertainty model prediction (*) with error bars to represent the predicted 3σ variation are shown with measured frequencies from six independent tests (×). Note that 9 of the 10 modes in these figures show significant variation in frequency. The variation is due partially to the gimbal nonlinearity discussed earlier and also to structural changes in the test article caused by disassembly and reassembly of the MBP between some of the tests.

Three of 10 frequencies (3.73, 39.56, and 49.67 Hz) show all measured frequencies within the predicted range of the uncertainty model; another 4 (2.26, 9.46, 16.11, and 17.84 Hz) give relatively close predictions; whereas 3 (25.05, 49.18, and 56.97 Hz) give poor predictions. Overall, however, the uncertainty model reduced the mean error of the frequencies, and some of the most important modes for control design (3.73, 9.46, 16.11, 17.84, and 39.56 Hz) fortuitously were predicted quite accurately. In addition, the more conservative and expanded bounds that cover both the mean and 3σ uncertainties predict the variations in all but the 49.18- and 56.97-Hz modes. Since the MACE flight, further work has improved the uncertainty modeling approach, yielding significantly better results.[23] However, the model presented here was the best available before flight.

Overall, the combined uncertainty model and mixed-μ analysis provided excellent results. Of the 130 preprogrammed controllers tested on orbit, only 7 destabilized the system. Of these seven, three were linear quadratic Gaussian controllers designed to emphasize the benefit of robust control and were predicted to be problematic. Several other controllers indicating possible problems ($\mu > 1$) did not destabilize the system, though many did show degraded performance in corresponding frequency ranges. This is consistent with the observation made earlier that the μ analysis can be conservative if the worst case perturbation does not occur. The remaining four controllers all destabilized the unmodeled low-frequency tether mode (0.14 Hz). Before flight, the possible use of tethers was assumed to introduce modes lower than 0.01 Hz. Therefore, tether modes were not included in the FE or uncertainty models, and all preprogrammed controllers were designed to roll up control authority above 0.01 Hz. The presence of a tether mode at 0.14 Hz was a surprise. Thus, the mixed-μ analysis failed for these four controllers, not because of any inherent deficiency in the technique, but rather because the uncertainty was not fully captured.

After the flight, the mixed-μ analysis was performed on controllers designed using the open-loop data analysis to compare the two techniques. The solid line in Fig. 7 is the upper bound on μ for one of the four measurement model controllers that destabilized the mode at 10 Hz. Note that $\mu > 1$ in four frequency regions, with the 10-Hz region being particularly troublesome. This indicates that the controller was not very robust, and thus it is not surprising that the actual system was destabilized. All four measurement-based controllers that destabilized the system showed similar analysis results. By contrast, the dashed line in Fig. 7 shows the upper bound on μ for the measurement-based controller that exhibited the best

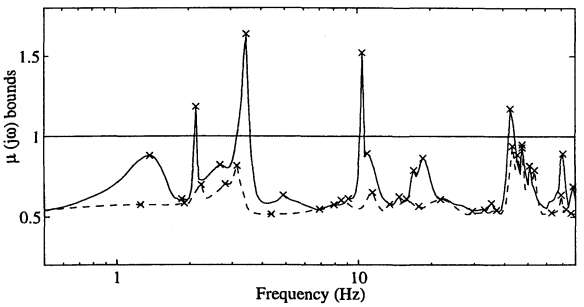

Fig. 7 Upper bound of μ as a function of frequency for two MM-based controllers redesigned during mission. The solid line had a 10-Hz instability, whereas the dashed line was the highest-performing design.

$\mathcal{H}_2$ performance. Because the upper bound is less than one over the entire frequency range, it is guaranteed that no perturbation within the uncertainty set can result in $\bar{\sigma}[S(j\omega)]$ more than twice ($\alpha = 2$) the nominal value. This indicates that robustness to frequency uncertainty is no longer the major factor limiting achievable performance. It also indicates that although three causes for excessive conservatism have been noted (calculation only of bounds, correlation of uncertainties, and expanded uncertainty set), the analysis is not so conservative that it limits controllers to much lower performance.

VI. Control Synthesis

Because of the support of the crew members on board STS-67, over 400 controllers were implemented on orbit. A complete summary of the closed-loop results is given in Ref. 9. This section gives a summary of the results pertinent to objectives 4 and 5 in the Introduction.

A. Control Problem Statement

The primary goal for the MACE control designs was to maintain precision two-axis inertial pointing of the primary payload while the secondary payload underwent scanning motions traceable to EOS-class (Earth Observing System) instruments. The performance metric consisted of the two-axis, rms pointing angle error between 0.5 and 50 Hz. A small penalty was also placed on the motion of the center node because a good control design should not only point the primary payload but also not excite the spacecraft bus. Therefore, a scalar performance cost was defined as a combination of all five integrated rate gyros (0.5–50 Hz) with a weighting of 1 for the two in the primary payload and 0.1 for the three at the center of the bus.

As noted earlier, four gimbal servocontrollers (from encoder to local gimbal) with a bandwidth (−3 dB) of one-tenth the first flexible mode were used as a nominal control design. This level of servocontrol was considered as standard industry practice because its bandwidth of 0.2 Hz avoided interaction with structural flexibility. To improve the inertial pointing over that achieved through standard industry practice, two control layers were applied. First, the bandwidth of the gimbal servos was increased to approximately 2 Hz. Second, multivariable robust control was implemented using the assortment of sensors and actuators on the test article. This second layer of control faced many challenging problems.

1) The test article contains 15 structural modes between 2 and 60 Hz.

2) The 1-g dynamics were strongly coupled to the gravity field and suspension system.

3) Achievement of over a factor of 60 improvement in pointing required substantial alteration of the disturbance-to-performance, input-output behavior.

4) Frequencies varied by as much as 5% between tests, whereas damping varied by as much as 100%.

5) Amplitude nonlinearity caused by friction and other structural effects caused some model parameters to vary substantially.

Each of these problems challenged the multivariable control design by requiring parameter robustness, rolloff in a dynamically rich frequency regime, development of high-order design models (up to 250 states), implementation of up to 80 state dynamic compensators, and prediction of behavior in an environment other than that in which

the MBP was tested. This control objective defined a problem that was challenging, traceable to other real world systems, and yet feasible for a secondary middeck experiment. The following discussion concentrates on the control results for configuration I. Other control design issues that were examined during the mission are listed in Table 2 and discussed in detail in Ref. 9.

B. Zero-Gravity Control Results for Configuration I

Figure 8 shows the (open- and) closed-loop performance plots for some of the best controllers implemented on orbit for configuration I. The scalar performance metric was defined previously as a combination of the five integrated rate gyros. Each controller used five inputs (two primary gimbal axes and three reaction wheels) and five sensors (two rate gyros in the primary gimbal and three reaction wheel axes). "Open Loop" refers to the standard industry practice servos, with a bandwidth set at one decade below the first flexible mode about each encoder, gimbal pair. "Servos Only" refers to a servobandwidth at approximately the first flexible mode. Figure 8 compares both preprogrammed (PP) and redesigned (RD) controllers based on the FE control design model. The preprogrammed controllers were analyzed using μ analysis and the predicted design and uncertainty models. Figure 8 shows that the best FE-model PP controller achieved a 31-dB (factor of 35) performance improvement over a broad frequency band significantly modifying the system dynamics up to approximately 30 Hz. The limiting factor in the preprogrammed designs was an unmodeled tether mode at approximately 0.14 Hz, which destabilized a higher-authority controller.

Controllers were redesigned during the mission using the FE model, but with stability and performance analysis based on measured on-orbit data. In addition, a frequency shape was added to the designs to avoid destabilizing the tether mode, while still achieving performance over the 0.5–50 Hz range. Figure 8 shows that the redesigned controllers improved performance up to approximately 20 Hz, resulting in a 35.2-dB improvement (factor of 58).

Figure 8 also shows the best measurement-model (MM)-based controller, which achieved a broadband improvement of 33 dB (factor of 45) in the payload pointing objective. This surpasses the performance improvement of the preprogrammed FE-model-based controllers but not the redesigned FE model controllers. This result is quite surprising because the original role of the identified model was to provide a measure of the performance degradation associated with the use of an analytic control design model.[24] Several redesigned MM-based controllers performed well in the data analysis but actually drove the z-axis dynamics unstable near 10 Hz. A variety of methods were used to compensate for what apparently were inadequacies in the data analysis. The postflight analysis discussed in Sec. V revealed that a large friction nonlinearity caused a 10-Hz gain discrepancy, thus destabilizing higher-authority controllers and limiting the attainable performance of the MM-based designs.

The significant improvement in relative pointing accuracy of the payload is graphically shown in Fig. 9, which compares the time domain response of the system in three cases: 1) open loop, 2) servos only, and 3) CST controller of the best FE-model-based redesigned controller (frequency response shown in Fig. 8). The x and z pointing angles are plotted for each case while two broadband disturbances (0–50 Hz) are applied to the secondary gimbal in each direction. These time histories show the dramatic reduction in pointing error as each layer of control was added.

Table 2 Primary control design issues for MACE

Design issue	Approaches considered
System configuration	Configurations I and II
Model fidelity	FE model, MM
Robustness analysis	Data and μ analysis
Uncertainty model	Parametric, data
Control design method	Classical, robust, narrowband, and $\mathcal{H}_2/\mathcal{H}_\infty$
Control topology	Feedback performance variable directly or not
Disturbance environment	Broadband, narrowband, and step-stare

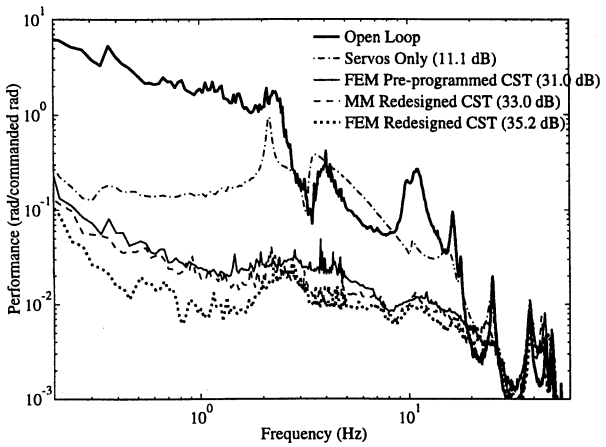

Fig. 8 On-orbit FE model and MM results for MACE configuration I.

C. Input Shaping

Input shaping is a strategy for generating time-optimal commands for controlled mechanical systems using only information about the problematic modes of vibration. This is similar in concept to feeding forward the disturbances to the control design because they are known commands. In this approach, shaped commands are created by convolving an actuator command with a series of impulses, called the input shaper. This impulse sequence can be derived by numerically solving a set of simple constraint equations or using a closed-form solution in some cases. A summary of the input shaping experiments performed on MACE is given in Ref. 10.

An example of a task that was studied during the MACE mission was understanding how to improve the performance of space systems containing multiple scanning or pointing payloads. This involved slewing the MACE secondary gimbal while a high-performance multivariable controller tried to maintain the pointing angle of the primary gimbal. A shaped or unshaped input command is sent to the z-axis secondary gimbal actuator servo while the absolute angular rate of the z-axis primary gimbal is measured. The controller used in this set of results was a medium-to-high-authority, measurement-model-based, robust controller, as described in Ref. 9.

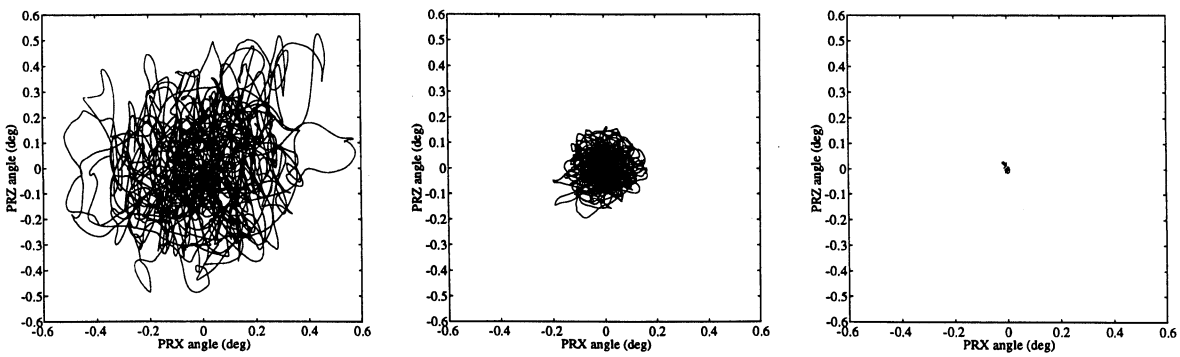

Open-loop **Servos only (11.1 dB)** **CST control (35.2 dB)**

Fig. 9 Pointing position with broadband disturbance.

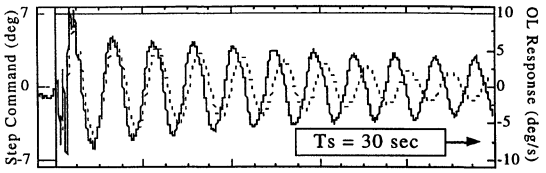

a) Open-loop response to a step command

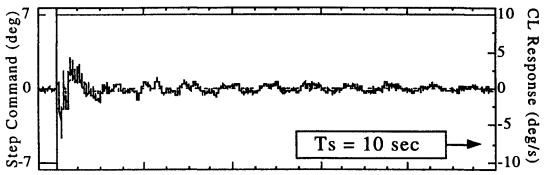

b) Closed-loop response to a step command

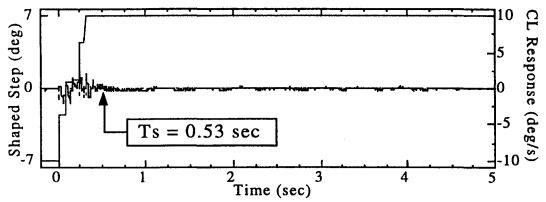

c) Closed-loop response to a shaped step command

Fig. 10 Input command (solid line starting at −7 deg at t = 0 with a steady state of 7 deg), experimental response (solid line oscillating about 0 deg/s), and predicted response (– – –) of the MACE configuration I, two-gimbal task for three different cases.

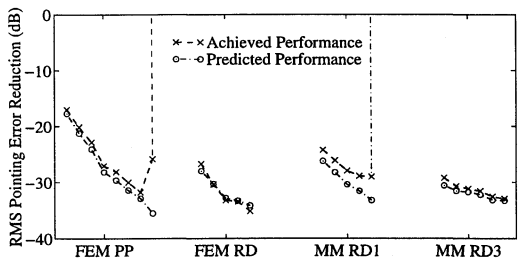

Fig. 11 Configuration I performance comparison: PP, preprogrammed, and RD, redesigned.

The input shaper used in these tests is a two-mode, zero-vibration shaper also designed during the mission using the flight data.

Figure 10 illustrates the time response of the primary gimbal while slewing the secondary gimbal for three different cases: 1) open-loop (servos only) response to a step command, 2) closed-loop response to a step command, and 3) closed-loop response to a shaped step command. The controller greatly reduces the vibration levels and settling time of the primary gimbal, but there are still residual vibrations in the first two lightly damped system modes (2.24 and 6.60 Hz). Consequently, when a two-mode shaper targeting these frequencies was added to the controlled system, the residual vibration and settling time was further reduced, as shown in Fig. 10c.

D. Closed-Loop Summary

The performance results from the MACE flight for configuration I are succinctly summarized in Fig. 11. This plot compares the predicted and actual closed-loop performance obtained using five-input/five-output compensators designed on both FE and measurement models and analyzed using a μ analysis for PP controllers and data analysis for RD controllers. Each curve corresponds to a set of compensators with increasing control authority. Predicted (o) and actual (×) performances are shown, where the predictions were obtained using the best model and analysis method available at the time of design.

The four main points from this plot are 1) the close agreement between the actual response and the predictions for most designs, 2) the performance improvements after the control redesigns, 3) the relative performance of the FE-model- and MM-based controllers, and 4) the ultimate performance levels obtained.

The closed-loop results of the FE-model PP controllers were quite good (up to 31 dB) and were predicted quite accurately except for the last controller, which destabilized the low-frequency (0.14-Hz) tether mode. The presence of the tether mode and its gradual deterioration in performance were the primary cause for the divergence of the prediction accuracy for the FE-model PP set. The redesigned FE-model controllers included a frequency shape on the control effort to avoid interaction with the tether mode and analysis based on the open-loop data. As a result, the FE-model RD controllers extended the performance improvement to 35.2 dB (38% improvement over FE-model PP), and the predicted performance matches the actual performance quite well for all cases. The limiting factors in these designs were phase loss and sensor noise.

The predictions of the first MM-based controllers (MM RD1), however, diverged with increasing authority, and the ultimate performance was less than the FE-based controllers. The final controller was one of four that destabilized the system at 10 Hz. The primary sources for the degraded performance and prediction were the presence of the nonlinearity (Fig. 5) and the use of one data set to create a measurement model and analyze controllers. The second redesign (MM RD2) had similar results. The MM RD3 controllers had the added benefit of a second set of measured data; therefore the predictions matched the actual results much better. In addition, the FE model was used to analyze the 10-Hz problem. The performance improvement increased to 33.0 dB (compared with the 28.9 dB of MM RD1) but was still lower than that obtained with the FE model. This problem is attributed to both a lack of design heritage (nine months for FE based, nine days for MM based) and the performance degradation associated with the conservative techniques used to avoid destabilizing the system at 10 Hz.

VII. Conclusions

A comprehensive evaluation of the leading model development and control formulations as applied to the control of precision spacecraft has been conducted by the Space Engineering Research Center at the Massachusetts Institute of Technology in conjunction with Payload Systems Incorporated, Lockheed Missiles and Space Company, and NASA Langley Research Center. The technology developed during the MACE program and demonstrated during the MACE mission satisfied each of the primary objectives.

1) The first objective was to understand how gravity affects the open- and closed-loop ground test results. Gravity can influence the entire structure (sag, predeformation, preloading) and components of the structure (articulating appendages, rigid-body behavior). Gravity and suspension also corrupt correlation between a structure's 0-g behavior and ground tests.

2) The second objective was to develop tools to predict the on-orbit behavior. Before the availability of on-orbit data, tools do exist (1-g FE model with data correlation and uncertainty modeling), which allow the development of 0-g models and reliable prediction of the remaining errors between these models and the actual dynamics in 0 g. These modeling tools can then be combined with an analysis tool (mixed-μ) to evaluate stability/robustness and to identify problematic parameters in the model. Using these tools, closed-loop controllers that achieve predictable closed-loop robust performance can be developed before flight.

3) The third objective was to quantify the accuracy to which the behavior can be predicted. For a system with 1- to 0-g frequency shifts up to 12%, the updated model predicted most 0-g frequencies to within 3% of their measured values. The uncertainty model predicted only 30% of the modes correctly. However, the overall modeling error was reduced, and subsequent methods performed significantly better. The mixed-μ test had a 97% success rate in predicting the stability of preprogrammed controllers. The 3% failure rate was due solely to unmodeled tether dynamics that were not included in the μ analysis. Controller performance prediction was found to be equally reliable. It is noted, however, that a second set of data for control analysis is important for the MM-based designs.

4) The fourth objective was to measure the open- and closed-loop behavior on orbit and to update the control system. On-orbit system ID is a very viable method for refining controllers. However, one must be careful to design the ID process to capture separate model development data as well as control evaluation data. In addition,

identification and modeling at different excitation amplitudes are suggested to help reveal nonlinearities that could be detrimental to the control designs. An on-orbit redesign was accomplished using data downlinks and uplinks, measurement model development, robust control design, and open-loop data analysis.

5) The fifth objective was to quantify the performance improvement that can be achieved through both prelaunch and on-orbit updated control designs. Both preprogrammed and on-orbit redesigned control enabled a factor of 60 improvement in pointing accuracy. Because operational systems may not allow the extensive model updating conducted for MACE, preprogrammed controllers can be relied upon for a factor of at least 10 improvement, whereas on-orbit redesign supplies the rest. An on-orbit redesign achieved 38% performance improvement over preprogrammed designs. In addition, input shaping can also be used to greatly reduce vibration for known command inputs.

These MACE flight results clearly illustrate that several components of the control-structures technology, such as the analytic model predictions, uncertainty modeling, performance analysis, and parametric robust control design techniques, performed very well during the mission and are useful tools for future spacecraft. The system identification process was shown to provide an excellent fit to the measured data, but the data were corrupted by nonlinearities that had not been experienced to such an extent during the ground tests. Several operational and communication constraints limited the ability to obtain and download additional open-loop data to determine the source of these nonlinearities during the mission. Nonlinearities, however, are a source of problems in real space hardware, especially in highly controlled, precision spacecraft. Therefore, system nonlinearities should be examined more closely in the identification, uncertainty modeling, and control design/analysis of the system. In addition, these factors suggest that including adaptive controllers that operate on orbit would be an important addition to the control-structures techniques validated on MACE.

In conclusion, these results summarize a very successful investigation of the modeling, analysis, and control design issues associated with a contemporary solution to the CSI problem. It is now hoped that these experimental on-orbit results will improve the confidence in these advanced techniques so that the tools can be applied to future spacecraft that cannot be tested on the ground in a sufficiently realistic 0-g environment.

References

[1]Crawley, E. F., and Hall, S. R., "The Dynamics of Controlled Structures," Space Engineering Research Center, TR SERC 10-91-I, Massachusetts Inst. of Technology, Cambridge, MA, July 1991.

[2]Ketner, G., "Survey of Historical Incidences with Controls-Structures Interaction and Recommended Technology Improvements Needed to Put Hardware in Space," Pacific Northwest Lab. (operated for the U.S. Dept. of Energy by Battelle Memorial Inst.), TR PNL-8646, Richland, WA, 1989.

[3]Nurre, G. S., Sharkey, J. P., Nelson, J. D., and Bradley, A. J., "Preservicing Mission, On-Orbit Modifications to the Hubble Space Telescope Pointing Control System," *Journal of Guidance, Control, and Dynamics*, Vol. 18, No. 2, 1995, pp. 222–229.

[4]Miller, D. W., Saarmaa, E., and Jacques, R. N., "Preliminary Structural Control Results from the Middeck Active Control Experiment (MACE)," *Proceedings of the AIAA Structures, Structural Dynamics, and Materials Conference*, AIAA, Washington, DC, 1992, pp. 566–576 (AIAA Paper 92-2138).

[5]Sparks, D. W., and Juang, J.-N., "Survey of Experiments and Experimental Facilities for Control of Flexible Structures," *Journal of Guidance, Control, and Dynamics*, Vol. 15, No. 4, 1992, pp. 801–816.

[6]Hyland, D. C., Junkins, J. L., and Longman, R. W., "Active Control Technology for Large Space Structures," *Journal of Guidance, Control, and Dynamics*, Vol. 16, No. 5, 1993, pp. 801–821.

[7]Glaese, R., and Liu, K., "On-Orbit Modeling and System Identification for MACE," *Proceedings of the IFAC 13th World Congress*, Vol. D, Elsevier Science, Oxford, England, UK, 1996, pp. 37–42.

[8]Grocott, S. C. O., and Campbell, M. E., "Control Analysis Results for MACE: Methods and Limitations," *Proceedings of the IFAC 13th World Congress*, Vol. D, Elsevier Science, Oxford, England, UK, 1996, pp. 43–48.

[9]Campbell, M. E., Grocott, S. C. O., How, J. P., and Woods-Vedeler, J. A., "Overview of Closed Loop Results for MACE," *Proceedings of the IFAC 13th World Congress*, Vol. D, Elsevier Science, Oxford, England, UK, 1996, pp. 49–54.

[10]Tuttle, T. D., and Seering, W. P., "Input Shaping Results from the MIT Middeck Active Control Experiment," *Proceedings of the IFAC 13th World Congress*, Vol. D, Elsevier Science, Oxford, England, UK, 1996, pp. 55–60.

[11]Miller, D. W., Sepe, R. B., Rey, D., and Crawley, E. F., "The Middeck Active Control Experiment (MACE)," *Proceedings of the 5th NASA/DOD CSI Technology Conference*, Scientific and Technical Information Program, Office of Management, NASA, Washington, DC, 1992, pp. 551–565.

[12]Glaese, R. M., and Miller, D. W., "Derivation of Zero-Gravity Structural Control Models from Analysis and Ground Experimentation," *Journal of Guidance, Control, and Dynamics*,Vol. 19, No. 4, 1996, pp. 787–793.

[13]Crawley, E. F., Barlow, M. S., van Schoor, M. C., Masters, B. P., and Bicos, A. S., "Measurement of the Modal Parameters of a Space Structure in Zero Gravity," *Journal of Guidance, Control, and Dynamics*, Vol. 18, No. 3, 1995, pp. 385–392.

[14]Rey, D. A., Crawley, E. F., Alexander, H. L., Glaese, R., and Gaudenzi, P., "Gravity and Suspension Effects on the Dynamics of Controlled Structures," *Proceedings of the AIAA Structures, Structural Dynamics, and Materials Conference*, AIAA, Washington, DC, 1993, pp. 3156–3171 (AIAA Paper 93-1662).

[15]Liu, K., Jacques, R. N., and Miller, D. W., "Frequency Domain Structural System Identification by Observability Range Space Extraction," *Journal of Dynamic Systems, Measurement and Control*, Vol. 118, No. 2, 1996, pp. 211–220.

[16]Grocott, S. C. O., How, J. P., and Miller, D. W., "A Comparison of Robust Control Techniques for Uncertain Structural Systems," *Proceedings of the AIAA Guidance, Navigation, and Control Conference*, AIAA, Washington, DC, 1994, pp. 261–271 (AIAA Paper 94-3571).

[17]Lehtomaki, N., "Practical Robustness Measures in Multivariable Control System Analysis," Ph.D. Thesis, College of Engineering, Massachusetts Inst. of Technology, Cambridge, MA, May 1981.

[18]Campbell, M. E., Grocott, S. C. O., How, J. P., Miller, D. W., and Crawley, E. F., "Verification Procedure for On-Orbit Controllers for the MIT Middeck Active Control Experiment," *Proceedings of the American Control Conference*, 1995, pp. 3600–3605.

[19]Young, P. M., Newlin, M. P., and Doyle, J. C., "μ Analysis with Real Parametric Uncertainty," *Proceedings of the IEEE Conference on Decision and Control*, Inst. of Electrical and Electronics Engineers, Piscataway, NJ, 1991, pp. 1251–1256.

[20]Balas, G. J., and Young, P. M., "Control Design for Variations in Structural Natural Frequencies," *Journal of Guidance, Control, and Dynamics*, Vol. 18, No. 2, 1995, pp. 325–332.

[21]Feron, E., "Analysis of Robust $\mathcal{H}_2$ Performance with Multipliers," *Proceedings of the IEEE Conference on Decision and Control*, Inst. of Electrical and Electronics Engineers, Piscataway, NJ, 1994, pp. 2015–2020.

[22]Paganini, F., "Necessary and Sufficient Conditions for Robust $\mathcal{H}_2$ Performance," *Proceedings of the IEEE Conference on Decision and Control*, Inst. of Electrical and Electronics Engineers, Piscataway, NJ, 1995, pp. 1970–1975.

[23]Campbell, M. E., and Crawley, E. F., "Development of Structural Uncertainty Models," *Journal of Guidance, Control, and Dynamics*, Vol. 20, No. 5, 1997, pp. 841–849.

[24]How, J., Glaese, R., Grocott, S., and Miller, D., "Finite Element Model Based Robust Controllers for the MIT Middeck Active Control Experiment (MACE)," *IEEE Transactions on Control System Technology*, Vol. 5, No. 1, 1997, pp. 110–118.

G. M. Faeth
Associate Editor